molecular pharmaceutics

Article

Cite This: Mol. Pharmaceutics 2019, 16, 173−183

pubs.acs.org/molecularpharmaceutics

In Situ Characterization of the Microstructural Evolution of Biopharmaceutical Solid-State Formulations with Implications for Protein Stability

Stijn H. S. Koshari,[†] Purnendu K. Nayak,[‡] Shalini Burra,[‡] Isidro E. Zarraga,[§] Karthikan Rajagopal,[∥] Yun Liu,[†,⊥] Norman J. Wagner,[†] and Abraham M. Lenhoff*[,†]

[†]Center for Molecular and Engineering Thermodynamics, Department of Chemical and Biomolecular Engineering, University of Delaware, Newark, Delaware 19716, United States

[‡]Eurofins Lancaster Laboratories Inc., Lancaster, Pennsylvania 17605, United States

[§]Late Stage Pharmaceutical Development and [∥]Drug Delivery Department, Genentech Inc., South San Francisco, California 94080, United States

[⊥]Center for Neutron Research, National Institute of Standards and Technology, Gaithersburg, Maryland 20899, United States

Supporting Information

ABSTRACT: Lyophilized and spray-dried biopharmaceutical formulations are used to provide long-term stability for storage and transport, but questions remain about the molecular structure in these solid formulations and how this structure may be responsible for protein stability. Small-angle neutron scattering with a humidity control environment is used to characterize protein-scale microstructural changes in such solid-state formulations as they are humidified and dried in situ. The findings indicate that irreversible protein aggregates of stressed formulations do not form within the solid-state but do emerge upon reconstitution of the formulation. After plasticization of the solid-state matrix by exposure to humidity, the formation of reversibly self-associating aggregates can be detected in situ. The characterization of the protein-scale microstructure in these solid-state formulations facilitates further efforts to understand the underlying mechanisms that promote long-term protein stability.

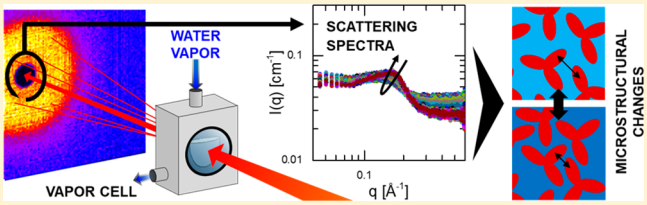

KEYWORDS: *lyophilization, spray-drying, monoclonal antibodies, vapor cell, small-angle neutron scattering, stability, protein−excipient microheterogeneity*

1. INTRODUCTION

Solid-state formulations of biopharmaceuticals, such as lyophilized or spray-dried proteins, are developed to provide protein stability during transport and long-term storage. Solid-state formulations are also used in drug-delivery systems as alternatives to the usual intravenous infusion or subcutaneous injection, like pulmonary delivery of powders or sustained drug-release devices such as polymer implants, microspheres, or solvent-depots.[1−5] However, the formation of protein clusters as irreversible aggregates is a prevalent form of instability in biopharmaceutical formulations, and the presence of such aggregates can have a negative impact on the drug's efficacy as well as lead to undesired immunogenicity and toxicity of the drug.[6]

To delay or prevent aggregation in the solid state, lyophilization and spray-drying are performed with stabilizers (such as sugars) and other additives (such as surfactants). While it is generally accepted that these stabilizers protect the protein from degradation in the solid state, the precise mechanism of stabilization is still an active topic of current research.[1,6−10] Though there has been significant work on the role of stabilizing sugars as a replacement for water molecules and on the molecular physics of the sugar, water, and amino acid interactions,[6,9] less is known about the protein-scale microstructure in these solid-state formations. This is especially relevant given that the protein molecules are in a highly crowded local environment as a result of the high protein concentration in the solid state, which can easily reach 50−80% by mass in typical formulations. In prior work, we elucidated the micron-scale protein heterogeneity of these formulations using confocal fluorescence microscopy,[11] where differences in protein heterogeneity suggested that a protein-scale microstructural investigation is warranted. To address these challenges, we demonstrate how protein-scale structure can be resolved in these formulations in situ by small-angle neutron scattering, where contrast between protein and excipients can be achieved by deuteration.

Received: September 5, 2018
Revised: November 18, 2018
Accepted: November 28, 2018
Published: November 28, 2018

DOI: 10.1021/acs.molpharmaceut.8b00935
Mol. Pharmaceutics 2019, 16, 173−183

Table 1. Overview of the Composition and Process Conditions of the Formulations Investigated

formulation	basic composition	sugar	S/P ratio	moisture content [%]	drying process	aggregate content [%]
F1	10 mg/mL mAb1; 4 mM L-His/HisHCl; pH 6.0; 0.01% (w/v) polysorbate 20	trehalose	1	<2	lyophilized	3.7−6.5
F2		deuterated sucrose	1	<2	lyophilized	/
F3		trehalose	1	<2	lyophilized	15.3 (heat-stressed)
F4	10 mg/mL Fab1; 10 mM L-His/HisHCl; pH 5.5; 0.01% (w/v) polysorbate 20	trehalose	1	3	lyophilized	1
F5		trehalose	1	7	spray-dried	1

Protein stability can be informed by the multiscale structural characterization of solid-state formulations, which encompasses knowledge of (1) the morphology and size of the solid-state particles, (2) the protein-stabilizer microheterogeneity, and (3) the presence of protein clusters or aggregates. Protein degradation has been shown to be more likely at the particle surface and is determined by the particle morphology, size, and protein distribution within the solid-state particles.[1,6,12−14] These factors also influence the reconstitution efficiency and the release rate during sustained drug-release applications.[2,5] Our previous research probed the three-dimensional morphology and protein-stabilizer microheterogeneity on particle (micrometer) length scales using confocal fluorescence microscopy (CFM).[11] That work demonstrated that, while particle-scale microheterogeneity is significant in spray-dried formulations, it is generally not observed in lyophilized formulations. Importantly, the observed microheterogeneity itself did not lead to an increase in irreversible aggregation in the formulations investigated, indicating that particle-scale microheterogeneity is not a sufficient condition for formulation instability. This is consistent with the expectation that the microheterogeneity on protein (nanometer) length scales, and not on particle length scales, is the most critical structural issue affecting protein stability. However, measuring molecular structural features on molecular length scales in situ in these solid-state formulations is extremely challenging. There is insufficient contrast between the protein and excipients for direct electron microscopy or X-ray scattering methods. However, the ability to selectively deuterate the sugars, or as is shown here, to introduce a controlled amount of deuterated water, provides a method to determine the average local protein environment via neutron scattering methods.

Small-angle neutron scattering (SANS) is well-suited to capture protein-scale structural information from these solid-state formulations, as it can probe features on nano- to micrometer length scales, is minimally disruptive (as opposed to X-rays), can penetrate opaque materials to determine internal structure, and can sample relatively large volumes.[15−19] Recently, SANS has been used to characterize the protein microstructure in solid-state formulations, mainly in the frozen state but also in lyophilized formulations of model proteins.[19−21] Scattering patterns show a single protein−protein interaction peak, which indicates a crowded amorphous morphology with average separation distances on the order of the protein molecular dimensions. Consequently, SANS has the potential to probe the protein aggregation and protein−excipient distribution in these systems. A distinct advantage of SANS over other methods is the ability to create scattering contrast between the proteins and excipients by isotopic labeling, uniquely enabling SANS to measure excipient and protein molecular distributions.[19]

Related but distinctly different techniques have recently been suggested as methods to predict the long-term stability of proteins in the solid-state, such as solid-state hydrogen−deuterium exchange with mass spectrometry (ssHDX-MS) and neutron backscattering (NB).[6,10,22−25] Similar to SANS, ssHDX-MS uses isotopic labeling to determine the amino acids that more readily exchange hydrogens upon exposure of the solid-state formulation to deuterated water vapor. These measurements have been shown to correlate with long-term stability, providing a potential route to predict formulation stability.[10,22,23] Similarly, NB probes the molecular dynamics of hydrogens in the formulation on fast time scales, and consistent with the prevailing thinking, faster molecular dynamics are implicated in limiting protein stability in the solid state.[6] While both of these methods show promise in predicting long-term stability by providing information about the molecular-scale dynamics, important questions remain about the protein-scale microenvironment in these solid-state formulations as well as about whether any small aggregates may be present in such formulations in the solid state.

Here we report a new method that exploits contrast variation and SANS to measure the protein-scale microstructure of several therapeutic monoclonal antibody (mAb) and antibody fragment (Fab) formulations in situ in the lyophilized or spray-dried state. In addition to identifying differences in structures of initially stable formulations, we have also investigated the effects of exposure to humidity and elevated temperature. An enhanced vapor cell SANS sample environment (VC-SANS)[26] was constructed that enables the measurement of the effects of cycling humidity on the protein-scale structure in situ. The resulting findings contribute to our fundamental understanding of protein behavior in solid-state formulations and highlight the potential of (vapor cell) SANS to further explore this behavior for different formulations and conditions.

2. EXPERIMENTAL SECTION

2.1. Materials. A recombinant humanized mAb of the IgG1 subclass (mAb1) and a model antibody fragment (Fab1) were manufactured by Genentech Inc. (South San Francisco, CA). Polysorbate 20 (PS20) was purchased from Spectrum Chemical Mfg. Corp. (Gardena, CA), trehalose dehydrate was purchased from Ferro Pfanstiehl Laboratories (Cleveland, OH), and fully deuterated sucrose ($C_{12}{}^2H_{14}H_8O_{11}$) was purchased from Omicron Biochemicals Inc. (South Bend, IN).

All formulations contained 10 mg/mL protein prior to drying, 0.01% (w/w) PS20, and 10 mg/mL of either trehalose or sucrose, which corresponds to a sugar-to-protein ratio (S/P) of 1. mAb1 formulations were prepared in 4 mM histidine/HCl buffer, pH 6, while Fab1 formulations were prepared in 10 mM histidine/HCl buffer, pH 5.5. An overview of the composition and process conditions of each sample is provided in Table 1. A heat-stressed formulation (F3) was obtained by maintaining a

DOI: 10.1021/acs.molpharmaceut.8b00935
Mol. Pharmaceutics 2019, 16, 173−183

regular lyophilized mAb1 formulation (F1) at 110 °C for 5 h. As an example of the particle-scale morphologies and protein distributions in typical lyophilized and spray-dried formulations, scanning electron microscopy (SEM) and confocal fluorescence microscopy (CFM) images of the two Fab1 formulations (F4 and F5), obtained as described previously,[11] are included in Figure 1. The spray-drying, lyophilization, moisture content

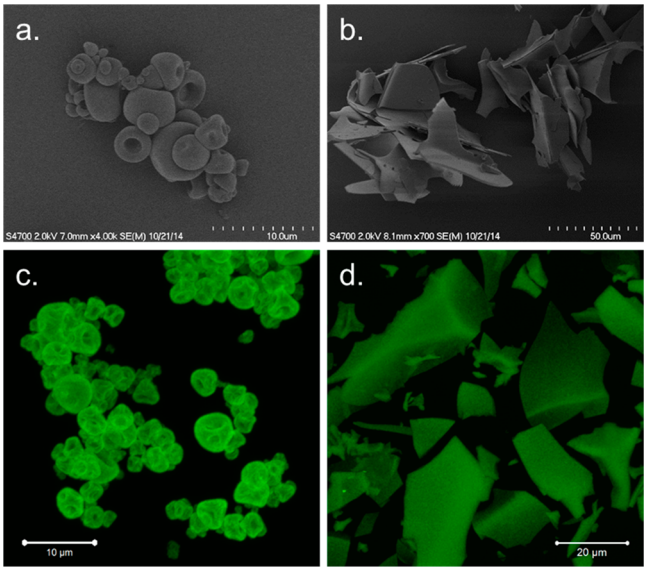

Figure 1. SEM (a,b) and CFM (c,d) images showing the particle-scale morphology and protein distribution of a spray-dried (Formulation F4: a,c) and a lyophilized (Formulation F5: b,d) Fab1 formulation.

determination, and size-exclusion chromatography (SEC) also follow the methodologies described previously[11] but are reiterated here for completeness.

2.2. Spray-Drying. The aqueous protein formulations were spray-dried using a B-191 mini Spray Dryer (Buchi, New Castle, DE) equipped with a 1 L cyclone particle separator to prepare micron-sized particles. The inlet temperature was set at 89 ± 2 °C, with 100% aspirator capacity at a 9.11 L/s gas flow rate. The atomizing air-flow rate was set at 19.66 L/min with a liquid feed rate of 3.4 mL/min. This resulted in an outlet temperature of 59 ± 2 °C. The spray-dried powder was collected in a clean dry glass vial and stored under vacuum until further use.

2.3. Lyophilization. The aqueous protein formulations were lyophilized in volumes of 0.5 mL in 2 mL glass vials in an SP Scientific Advantage Pro lyophilizer (Gardiner, NY). The lyophilization cycle was run with conservative drying settings known from experience to produce acceptable lyophilized material. The freezing shelf temperature and freezing rate were set at −35 °C and 0.3 °C/min, respectively. The primary drying temperature and chamber pressure were −20 °C and 100 μm Hg, respectively. The primary drying time was determined from the differential pirani/capacitance measurement. The secondary drying temperature, chamber pressure, and drying time were 25 °C, 100 μm Hg, and 10 h, respectively. The ramp rates between drying steps were 0.2 °C/min, and the headspace pressure was 760 mmHg. This lyophilization process typically produces solid cakes with moisture content of less than 1%. Solid cakes were manually broken up to allow loading into the SANS sample cell.

The glass transition temperature (T_g) of the lyophilized formulations was measured by modulated differential scanning calorimetry (MDSC, TA Instruments Q2000, New Castle, DE). Approximately 1−3 mg of sample and an empty reference pan were sealed in a TA hermetical aluminum pan. The MDSC experiments were performed by equilibrating the samples and reference pan to 5 °C for 10 min, modulating ±1 °C every 60 s, and then heating to 200 °C at a rate of 2 °C/min. The T_g was determined as the glass transition midpoint in the reversing signal and was found to be 120 °C for the lyophilized mAb1 formulations with trehalose (F1 and F3, Table 1).

2.4. Moisture Content Determination. The moisture content of the spray-dried and lyophilized formulations was determined by a Coulometric Karl Fischer (KF) titrator (Mettler-Toledo C30, Columbus, OH) equipped with a diaphragmless electrode and solvent manager. Approximately 30 mg of spray-dried/lyophilized sample was weighed into vials, to which 0.5−1 mL of methanol was added to extract the moisture from the samples. The samples were held for 10 min before starting the potentiometric titration. To start the analysis, the samples were injected into the titration cell with Hydranal Coulomat Water Standard (Sigma-Aldrich, St. Louis, MO). The sample injection was done manually using a Hamilton Syringe (Sigma-Aldrich) with a 20G needle, and the analysis was performed using Mettler-Toledo-Software LabX 2014. The results of this analysis are included in Table 1.

2.5. Size-Exclusion Chromatography. Size-exclusion chromatography (SEC) was performed on a TOSOH TSK-Gel Super SW3000 (7.8 × 300 mm) column using an Agilent 1200 series HPLC system equipped with a diode array detector (DAD). Samples were eluted at 30 °C in isocratic mode with 0.20 M K_3PO_4, 0.25 M KCl, pH 6.2 as the mobile phase at a flow rate of 0.5 mL/min. Prior to analysis, samples were diluted to approximately 1.0 mg/mL in water, and 100 μL of sample was injected. The total run time was 30 min, and absorbance at 280 nm was used for detection of the SEC peaks, which were classified as monomer, high molecular weight species (HMWS) or aggregates, and fragments. The percent peak area at 280 nm was calculated by dividing the peak area of each group at each time point by the total peak area. The results of this analysis are included in Table 1.

2.6. Small-Angle Neutron Scattering. An extensive overview of the theoretical background on small-angle neutron scattering (SANS), with particular regard to its use for solid-state protein systems, has been provided in prior work.[19] Briefly, SANS measures the scattering intensity $I(q)$ as a function of the magnitude of the momentum transfer vector q, which is related to the angle of deflected neutrons from the incident beam, θ, as[16−18]

$$q = \frac{4\pi}{\lambda}\sin\frac{\theta}{2} \quad (1)$$

where λ is the wavelength of the neutrons. The scattering intensity arises from structural heterogeneities between materials with differences in neutron scattering length density (SLD), ρ; the SLD is material-dependent and determines the scattering contrast in the sample. As q is related to the length scale being probed, d, by Bragg's law[16]

$$d = \frac{2\pi}{q} \quad (2)$$

features observed in SANS patterns contain structural information on the sample on these real-space length scales.

Because the SLD of a typical protein and sugar are similar, structural features of proteins within a sugar matrix are generally not observed by SANS (Figure 2). However, as proteins and

DOI: 10.1021/acs.molpharmaceut.8b00935
Mol. Pharmaceutics 2019, 16, 173−183

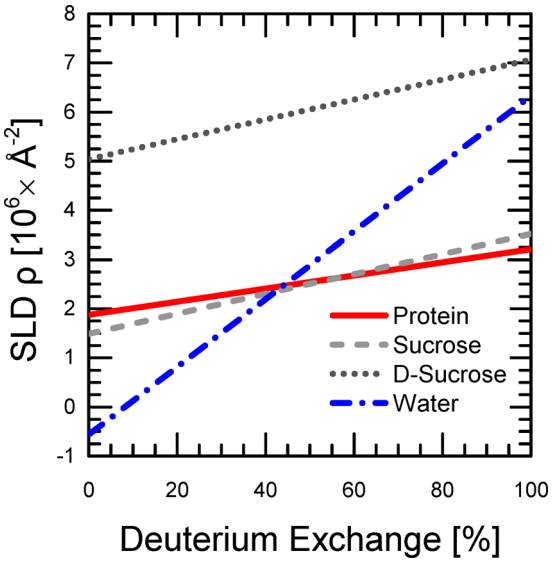

Figure 2. Schematic of the different neutron scattering length densities (SLDs) of a typical mAb, sucrose, fully deuterated sucrose, and water as a function of the amount of deuterium exchange of exchangeable hydrogens of each molecule.

sugars contain exchangeable hydrogens, the SLD is a function of the extent of deuterium exchange. Figure 2 illustrates that there are two straightforward methods to increase the contrast for a specific formulation: (1) use deuterated sugars (or proteins) and (2) introduce deuterium oxide (D_2O) into the system. Both methods are used in this work and provide complementary information.

The experiments were carried out on the 10 m NGB (nSoft) SANS instrument at the NIST Center for Neutron Research (NCNR), National Institute of Standards and Technology (NIST), Gaithersburg, MD. The instrument settings for the tests were

- high q: 1.2 m sample-to-detector distance (SDD) with 5 Å neutrons for a 600 s count time
- intermediate q: 4.5 m SDD with 5 Å neutrons for a 1200 s count time
- low q: 4.5 m SDD with lenses with 10 Å neutrons for a 1500 s count time

When spliced together, these regions result in a scattering range of 0.004 $Å^{-1} < q < 0.6$ $Å^{-1}$, corresponding to length scales ranging from approximately 1600 to 10 Å. The wavelength spread was 0.15 for all samples.

For time-resolved vapor cell studies, data were collected in time bins of 360 s at the high-q instrument setting, with intermittent full-range scans approximately every 4.5 h to probe the structural integrity of the samples. Sample cells with demountable quartz windows and a path length (thickness) of 1 mm were used for static experiments, while the NIST vapor cell described below was used for all time-resolved experiments. Standard data reduction procedures were followed to reduce the data to circularly averaged patterns.[27]

2.7. Vapor Cell. The vapor cell used at NIST consists of a titanium cell with quartz windows, as shown schematically by Shelton et al.[26] The setup of the vapor cell SANS experiment is depicted in Figure 3. The cell has a vapor inlet at the top and a vapor outlet at the bottom, allowing vertical vapor flow through the sample chamber, and it can be temperature-controlled from approximately 5 to 90 °C. The cell is connected to a nitrogen

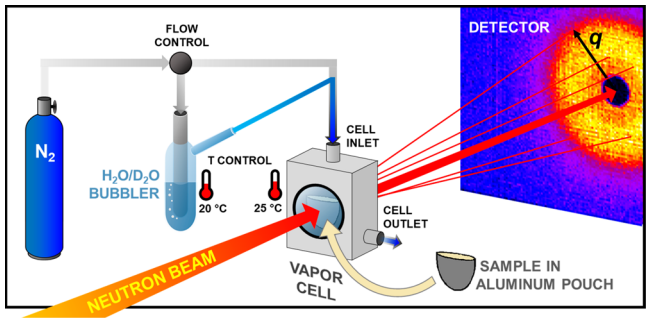

Figure 3. Schematic of the vapor cell setup at the NCNR.

source via a flow path that can be toggled to allow flow through or to bypass a bubbler filled with water. The bubbler is held at 20 °C, while the vapor cell is at 25 °C to prevent vapor condensation in the connecting lines and vapor cell. The sample powders were mounted into the sample chamber within an aluminum foil pocket, which was open at the top to allow vapor exchange with the sample chamber. Samples were exposed to either a continuous pure nitrogen (N_2) gas flow or a mixed D_2O–N_2 or H_2O–N_2 vapor flow for periods of several hours, while the SANS patterns were collected in time bins of several minutes.

3. RESULTS AND DISCUSSION

The nanoscale microstructures of five different solid-state monoclonal antibody (mAb) and antibody fragment (Fab) formulations, listed in Table 1, were investigated using small-angle neutron scattering (SANS). The static microstructure of the formulation was first probed using regular SANS, and then microstructural changes under the influence of water uptake were investigated using SANS in a vapor cell environment (VC-SANS). Quantitative agreement was observed between the initial structures measured in the standard demountable cells and in the VC-SANS cell.

3.1. Static Microstructure. A typical SANS pattern of a solid-state biopharmaceutical formulation, represented by Formulation F1, is shown in Figure 4 (blue). The pattern shows flat background scattering at high q-values (small-length scales) and power-law behavior, with a slope of −4, at small q values. This Porod slope indicates scattering from the sharp surface of the micron-sized particles that comprise the solid formulation. In the case of a lyophilized formulation, these are the thin plate-like particles resulting from the crushing of the lyophilized cake, while for a spray-dried formulation, these are the hollow spherical particles as observed by confocal fluorescence microscopy (Figure 1).[11] The background evident at high q is a result of incoherent scattering that arises mainly from hydrogen atoms.

The scattering pattern of the typical formulation without deuteration lacks any features that correspond to the internal structure of the dried powders—the structure of protein molecules distributed in the excipient—because of the lack of contrast between the excipient and the protein (Figure 2). Figure 4 shows that using fully deuterated sucrose as an excipient in Formulation F2 enhances the contrast between the protein and the sugar phase sufficiently to obtain protein-scale structural information from SANS. Here this structural information appears in the form of a single broad peak at intermediate q values.

DOI: 10.1021/acs.molpharmaceut.8b00935
Mol. Pharmaceutics 2019, 16, 173−183

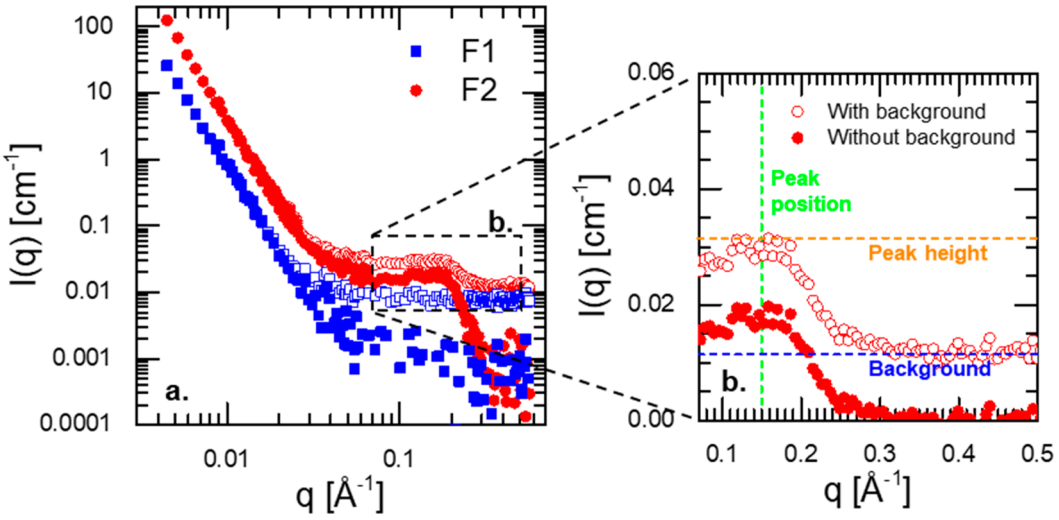

Figure 4. Comparison of SANS patterns of a lyophilized mAb1 sample in regular (F1) and deuterated (F2) sugar (a) and overview of prominent scattering metrics reported in the time-resolved experiments (b). Open symbols show the scattering patterns before subtraction of the incoherent scattering background, while filled symbols show the patterns after subtraction. The dashed box indicates the area of the pattern highlighted in the time-resolved vapor cell experiments (Figure 5).

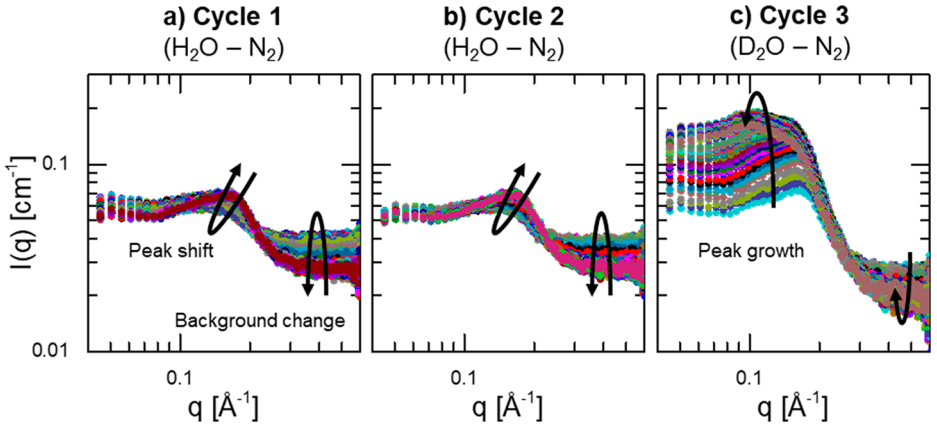

Figure 5. Evolution of the SANS pattern of lyophilized mAb1 in deuterated sucrose (F2) as a function of time under cycles of alternating nitrogen and water vapor flows. The arrows on the scattering pattern indicate the general trend of the pattern with time. A video of the evolution of the SANS patterns with time is included in the Supporting Information.

Such a peak has been observed before in lyophilized formulations of model proteins such as lysozyme as well as in frozen mAb formulations and is characterized as a nearest-neighbor peak or a protein−protein interaction peak, because the peak position corresponds to the average protein−protein distance in the amorphous formulation.[19−21] In Figure 4, the observed peak position of 0.15 Å^{-1} corresponds to an average protein−protein center-to-center separation distance of d = 42 Å (eq 2). As the radius of gyration (R_g) of a mAb is approximately 50 Å, and mAbs are highly anisotropic, mAbs must orient favorably and interdigitate to pack with the observed separation distance in these solid formulations.[20,28] However, comparison to SANS measurements of frozen mAb formulations without sugars,[19] where d = 31 Å, indicates that the mAbs are separated by the stabilizers. These measurements show that the presence of sugar in this formulation leads to an increase in the average protein−protein surface separation distance of ∼11 Å, which is comparable to the molecular size of trehalose ∼9 Å.[29] Thus, our measurement confirms the assumption of the sugar forming a protective adsorbed layer surrounding the protein in these solid formulations.

Although the use of deuterated sucrose in the formulation clearly increases contrast sufficiently to show structural features of the protein in the sugar matrix, it does not alter the power-law scattering in the low-q regime. Consequently, there are no significant microstructural features in the corresponding range of 300 to 1600 Å, such as distinct protein-rich clusters or other microheterogeneities. The longest length scales probed by SANS are comparable to the limit of resolution of the confocal fluorescence microscopy imaging performed previously for similar formulations,[11] which is approximately 1500 Å or 0.15 μm. Hence, we conclude that mAbs in these lyophilized formulations are distributed uniformly on length scales from that of the protein to that of the particle, and that there are no microheterogeneities or evidence of any significant population of aggregated protein.

3.2. Microstructural Changes under Cyclic Humidification. These results show that SANS is a promising method to study the microstructure of therapeutic proteins in a variety of formulations with different process conditions, compositions, and protein stability. However, the use of deuterated excipients requires modifications to the standard formulations and may

DOI: 10.1021/acs.molpharmaceut.8b00935
Mol. Pharmaceutics 2019, 16, 173−183

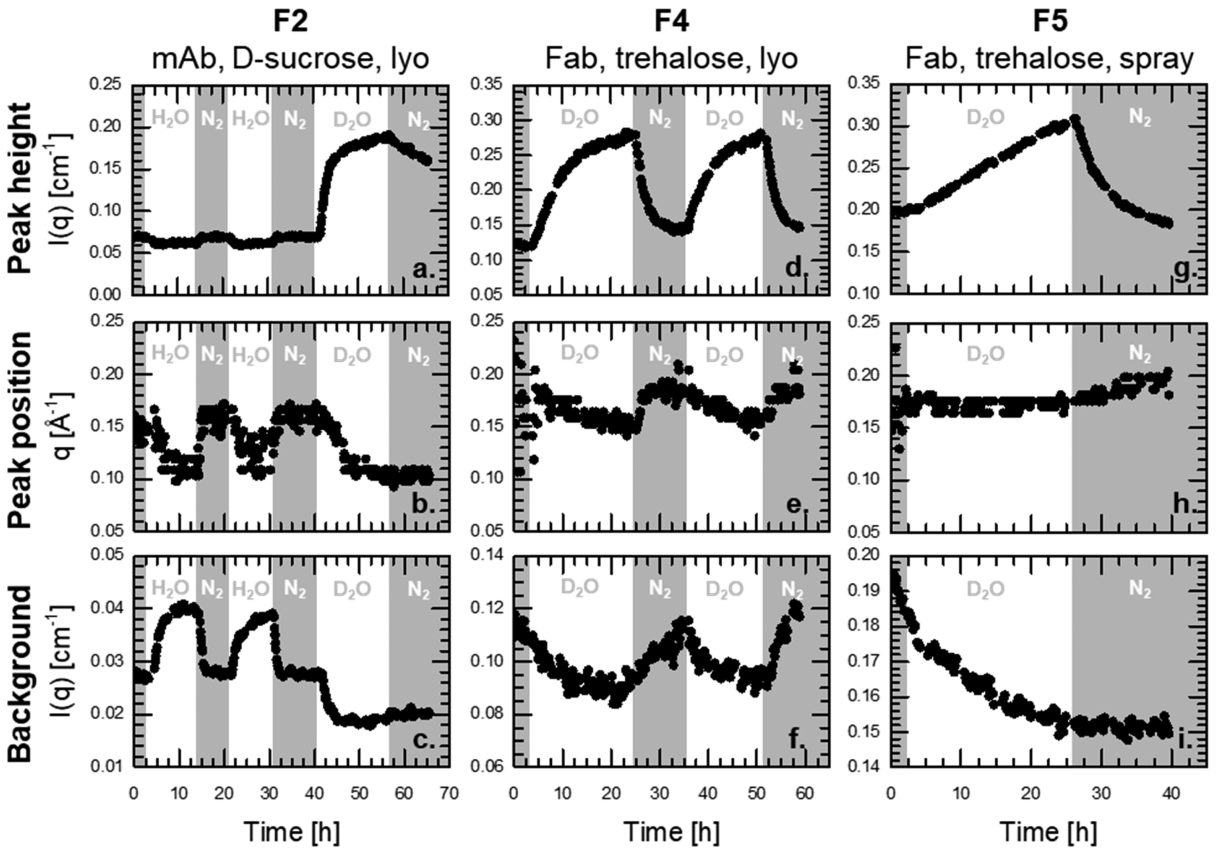

Figure 6. Evolution of prominent scattering features of three formulations as a function of time under cycles of alternating nitrogen and water vapor flows.

lead to changes in protein−excipient interactions. Another way to introduce contrast in solid-state formulations is by introducing D_2O into the formulation through uptake from the vapor phase. The D_2O will diffuse through the hygroscopic powder, mainly in the sugar phase, and increase the SLD contrast. In addition, it will lead to deuterium exchange with exchangeable hydrogens on both the protein and sugar, which will occur as a function of time and exposure. For example, hydrogens in the core of the protein will not exchange as rapidly as those readily accessible on the sugar molecules, an effect that has recently been exploited to study protein formulation stability.[10,22,23,30] In the following, we exploit this method to further study the protein−excipient distribution in these solid-state formulations.

The advantage of using the vapor cell in this manner is twofold. First, the uptake of D_2O within the sample greatly enhances the contrast, allowing the observation of the microstructure, i.e., the protein−protein interaction peak, in typical solid-state samples without the use of deuterated sugar. Second, the vapor cell allows in situ characterization of microstructural changes under stressed environmental conditions such as heat or water uptake. Formulations in the vapor cell were initially exposed to pure nitrogen flow for a period of about 1 h to ensure the removal of excess water. Subsequently, formulations were exposed to cycles of alternating nitrogen and water vapor flow, while their microstructural changes were monitored using SANS.

The evolution of the SANS patterns with time for the deuterated sucrose formulation (F2) for three successive water vapor−nitrogen cycles is shown in Figure 5. As the use of deuterated sugar provides sufficient contrast to distinguish the nearest-neighbor peak, the effects of moisture uptake and contrast changes because of the introduction of deuterium can be decoupled. Specifically, H_2O vapor can be used to investigate the effect of humidity and moisture uptake on the formulation, while D_2O vapor can be used to investigate the changes in contrast. In general, exposure to water leads to distinct changes in the scattering patterns over time that can be characterized by three main metrics: the peak height, the peak position, and the background scattering (Figure 4b). Changes in peak height can be attributed to the number of available scattering objects (protein molecules) and the contrast between the protein and excipient components. Changes in peak position can be attributed to changes in the interprotein distance or protein distribution. Lastly, changes in background scattering can be attributed to the amount of hydrogen present in the formulation and hence the uptake of hydrogenated water.

The evolution of these three structural metrics throughout the progress of the vapor cell experiment is shown in Figure 6a−c. The exposure to H_2O is expected to lead to an increase in the background scattering, as additional water is taken up by the hygroscopic powder. In addition, uptake of H_2O is expected to decrease the contrast in the sample if H_2O distributes throughout the sugar phase. This can be understood from Figure 2, where, in the case of no deuterium exchange, mixing of water (SLD below that of the protein) with the deuterated sugar (SLD above that of the protein) will effectively reduce the SLD of the sugar component and decrease the SLD difference between the sugar and protein. Indeed, Figures 5a and 6a,c show that the peak height decreases and the background increases

DOI: 10.1021/acs.molpharmaceut.8b00935
Mol. Pharmaceutics 2019, 16, 173−183

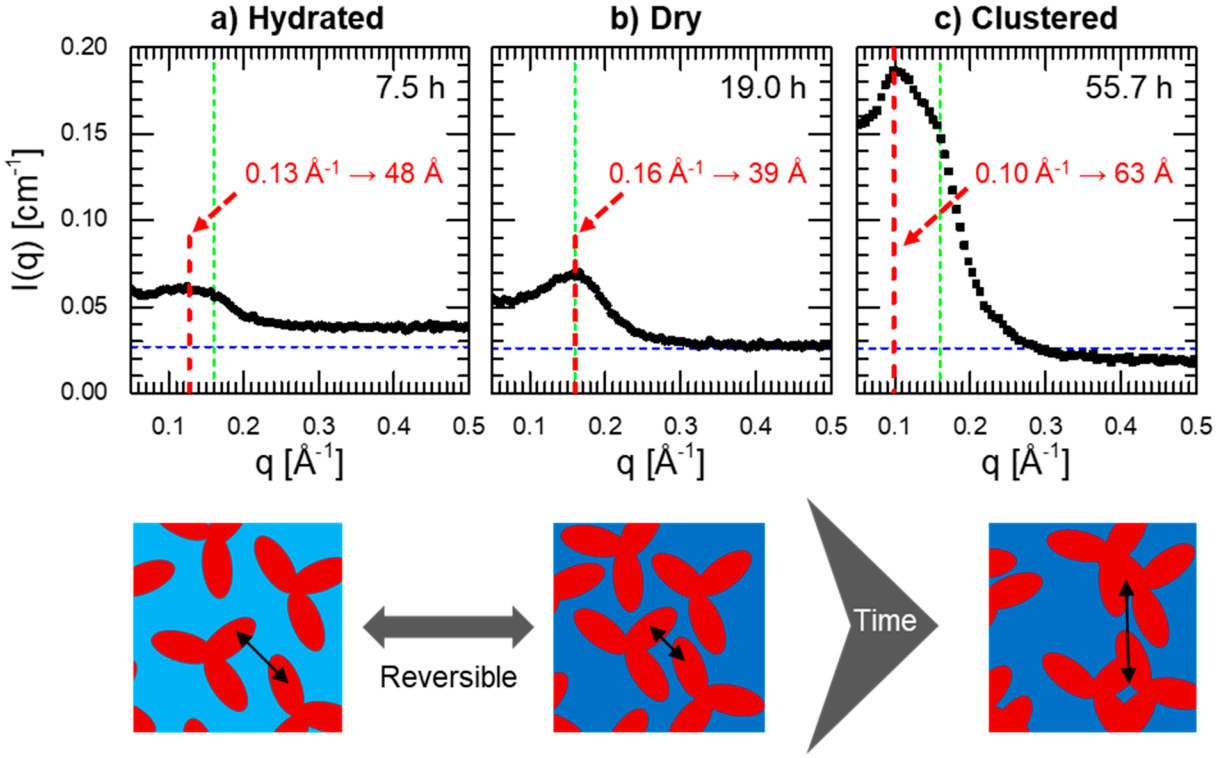

Figure 7. Overview of observed peak positions of lyophilized mAb in deuterated sugar (F2) with schematics of the corresponding hypothesized microstructures. The green line indicates the original peak position, while the blue line indicates the original background value.

with H_2O uptake over a period of 10 h. Subsequent drying of the samples with N_2 reverses this effect.

The uptake of H_2O also has a significant effect on the peak position and hence on the average protein−protein distance within the formulation. Upon the introduction of water, the nearest-neighbor peak gradually moves to smaller q values, corresponding to an increase in the average interprotein distance (Figure 5a). Thus, the sample swells upon humidification at the level of interprotein separation. Upon subsequent drying with nitrogen, this distance is observed to recover, but it recovers to an average separation distance slightly smaller than that in the original formulation. The corresponding scattering patterns at the two distinct peak positions are shown in Figure 7a,b, with approximate peak positions and average protein−protein distances listed in Table 2. This shows that the drying rate and conditions, i.e., processing, influence the formulation at the nanometer scale.

Table 2. Overview of SANS Peak Positions for mAb and Fab Formulations[a]

	F2: lyophilized mAb1	F4: lyophilized Fab1	F5: spray-dried Fab1
initial peak	0.15 $Å^{-1}$	0.17 $Å^{-1}$	0.17 $Å^{-1}$
	42 Å	37 Å	37 Å
hydrated peak	0.13 $Å^{-1}$	0.16 $Å^{-1}$	0.17 $Å^{-1}$
	48 Å	39 Å	37 Å
dry peak	0.16 $Å^{-1}$	0.18 $Å^{-1}$	0.19 $Å^{-1}$
	39 Å	35 Å	33 Å
cluster peak	0.10 $Å^{-1}$	/	/
	63 Å		

[a]The characteristic distance is estimated from the q-value using Bragg's law (eq 2).

The uptake of water in solid-state formulations is known to decrease the glass transition temperature (T_g).[9] Here, the formulations are subjected to very high humidity levels, which plasticizes the sugar−protein matrix. Indeed, the formulation powders are visibly collapsed after the vapor cell experiment, leading to densification of the powder. Regardless, regular full scans of the scattering patterns throughout the course of the vapor cell experiment show the same scattering from larger particles at low q values, indicating that the powders retain their solid morphology (data included in Supporting Information). However, as shown, water uptake leads to sufficient plasticization to "swell" the matrix between protein molecules, while drying leads to an average separation distance that is slightly smaller than in the original formulation (bottom panels of Figure 7a,b). The fact that the peak shifts gradually over several hours suggests that these microstructural changes occur throughout the whole sample volume to approximately the same degree. Importantly, repeating this H_2O−N_2 cycle leads to identical changes in the scattering patterns, indicating that the process is reversible (Figures 5b and 6a−c).

Using D_2O instead of H_2O vapor is expected to lead to similar morphological changes but with a significant change in the scattering intensity because of the increase in contrast. Moreover, the background scattering is expected to decrease as hydrogen is removed from the system because of deuterium exchange. This is indeed observed, where upon D_2O uptake, the peak height increases substantially while the background scattering decreases (Figure 5c). Initially, the peak position moves to smaller q values just as during H_2O uptake. However, after a few hours of exposure, a separate, second peak emerges at even smaller q values (Figure 6a−c).

This second peak is hypothesized to be the result of scattering from protein clusters or (reversible) aggregates in the formulation. Hence, the position of this cluster peak represents

DOI: 10.1021/acs.molpharmaceut.8b00935
Mol. Pharmaceutics 2019, 16, 173−183

the average distance between protein clusters or a protein cluster and a monomer and not between individual molecules (Figure 7c, bottom). There are several factors that support this hypothesis. First, the fact that the second peak emerges independently of the first peak and does not involve a shift of the first peak indicates that the peak is caused by a distinct fraction of protein molecules in the formulation, which grows over time, and not a general change in the protein microstructure as seen during water uptake and release. Second, the rapid growth of the second peak, without a similar decrease in the first peak, supports the viewpoint that the protein indeed forms correlated clusters. This idea is based on neutron scattering theory, which states that, if changes to the particle structure and interactions are neglected, the total scattering intensity increases 2-fold if two smaller particles merge.[17] Third, the position of the peak, which at 0.10 $Å^{-1}$ corresponds to an average separation distance of 63 Å, is consistent with the radius of gyration of a mAb dimer, assuming that the dimers interdigitate similarly to the mAb monomers. The radius of gyration of mAb dimers in concentrated solutions has been measured by SANS as 69 Å.[28]

Interestingly, some mAbs have been shown to form reversible dimers in solution that coexist with the dispersed monomers, even at relatively low concentrations.[28,31] In the solid state, the formation of such dimers could occur as a function of time in the plasticized state or could be triggered specifically because of the presence of D_2O, which can alter interactions among protein, water, and excipients. In either case, these findings show that such dimers form even in the solid state when sufficient mobility of the mAb is possible as a result of plasticization of the matrix.

3.3. Comparison between mAbs and Fabs. The VC-SANS patterns of a lyophilized formulation containing a Fab and regular, nondeuterated sugar (Formulation F4) were used to assess whether the increase in scattering contrast because of D_2O exposure is sufficient to reveal the protein microstructure in such nondeuterated formulations as well as to characterize potential differences between the microstructures of mAbs and Fabs. The evolution of key metrics of the SANS patterns of Formulation F4 is shown in Figure 6d–f, and a video of the evolution of the patterns with time is included in the Supporting Information. Initially, the patterns of this nondeuterated formulation are similar to that of Formulation 1 in Figure 4, with no indication of the nearest-neighbor peak. However, exposure to D_2O vapor increases the contrast sufficiently to reveal a single scattering peak. Consequently, VC-SANS is a promising technique to investigate the protein-scale microstructure of pristine biopharmaceutical formulations.

The exposure to water vapor can modify the microstructure, as evidenced by the changes in peak position and visible densification of the powder, which can compromise the ability of VC-SANS to reveal the true, native particle microstructure. However, the plasticization of the matrix is primarily the result of the high relative humidity in the vapor cell. Previous work on hydrogen–deuterium exchange in solid-state biopharmaceutical formulations (ssHDX) has shown that a lower relative humidity, below approximately 11%, can lead to deuterium exchange while keeping the powder density intact.[10] While we did not pursue such low levels of humidification here, continued studies along the lines of those presented here but at low relative humidity could aid in investigating the native microstructure of nondeuterated biopharmaceutical formulations.

While the nearest-neighbor peak of the lyophilized Fab formulation follows similar trends to those of the mAb formulation during water uptake and release, the peak positions naturally correspond to smaller protein–protein distances (Table 2), consistent with the smaller size of Fabs (R_g of 28 Å). Moreover, unlike the packing in the highly anisotropic mAbs, the globular Fabs do not interdigitate, and the Fab R_g is smaller than the average protein–protein distance in all cases, which corresponds to the behavior of globular proteins more generally.[20] Although this Fab1 has a similar microstructure to the Fab of mAb1, a second peak does not appear in the scattering patterns, so we can conclude that they do not form dimers or other aggregates within the time scale of the experiment.

3.4. Comparison between Lyophilization and Spray-Drying. Lyophilization and spray-drying are vastly different drying processes, which lead to very different particle morphologies as well as differences in protein–excipient microheterogeneity on the particle scale.[11] For example, certain spray-dried formulations show an increase in protein concentration toward the exterior of the particles, while proteins in lyophilized formulations are generally homogeneously distributed on the particle scale (Figure 1). To investigate the effects of the drying method on the protein-scale microstructure, the VC-SANS patterns of a lyophilized (Formulation F4) and a spray-dried (Formulation F5) Fab formulation in a nondeuterated sugar are compared, where both have the same nominal sugar-to-protein ratio of 1.

Despite the different drying mechanisms, the protein-scale microstructure of lyophilized and spray-dried formulations is similar, as shown by the evolution of key metrics of the SANS patterns of Formulations F4 and F5 in Figure 6d–i. While the average protein–protein distance is slightly smaller in the spray-dried formulation (Table 2), overall trends in the scattering patterns are maintained. In a solid-state formulation containing microheterogeneity, with certain areas enriched in protein and others depleted, it is expected that the local, average protein–protein distance will be smaller than for the situation where the same amount of protein is homogeneously distributed. Hence, the smaller average protein–protein distance in the spray-dried formulation is consistent with the particle-scale microheterogeneity observed in CFM (Figure 1). Moreover, the full q-range SANS patterns (included in the Supporting Information) show that this microheterogeneity in the spray-dried formulation does not originate from major changes in protein-scale microstructure but rather can occur by a redistribution of the excipient between the protein molecules.

This observation raises a question about how the microstructure is affected when insufficient sugar is present to stabilize the protein, either throughout the whole formulation or locally because of microheterogeneity. Below a certain sugar-to-protein ratio, which depends on the specific sugar, protein, and overall formulation conditions, formulations can exhibit a loss of protein stability.[9] As all of the formulations in this study are initially stable, with sugar-to-protein ratios of 1, it is expected that adequate sugar will be present and that the effects of low sugar-to-protein ratios are not probed with these formulations. However, the methodology developed here can be applied to study such formulations with low sugar-to-protein ratios as well as other solid-state formulations.

3.5. Relation between Microstructural Changes and Aggregation. The VC-SANS results can be used to assess the effects of the protein-scale microstructural changes in the solid-state formulations on the aggregation behavior and stability of the protein. As SANS probes the ensemble microstructure over the whole sample volume, it is better suited to studying the

DOI: 10.1021/acs.molpharmaceut.8b00935
Mol. Pharmaceutics 2019, 16, 173–183

mechanisms and structure of bulk aggregation events than to detecting small degrees of protein aggregation. While this study focuses on initially stable formulations, where aggregate formation over the lifetime of the formulation is expected to be limited, interesting aspects of the aggregation mechanisms are revealed by observation of the microstructural changes in stressed conditions, such as through exposure to humidity and high temperature.

The evolution of the nearest-neighbor peak height in the VC-SANS patterns of both an unstressed (F1) and a heat-stressed (F3) formulation under D_2O flow is included in Figure 8. To

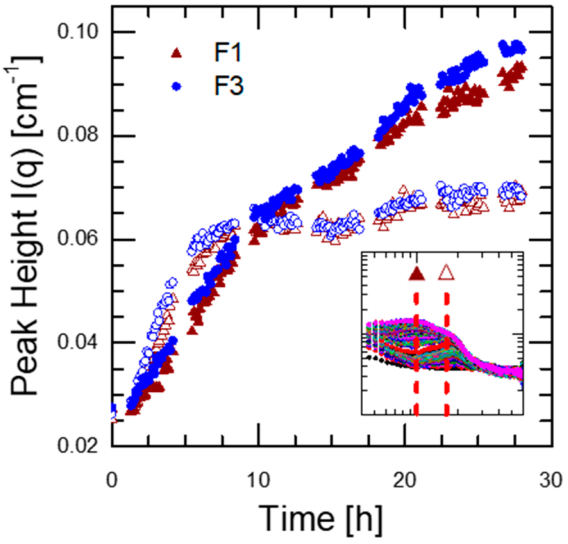

Figure 8. Comparison of peak height evolution over time during exposure to vapor cell D_2O flow for a regular (F1) and a heat-stressed lyophilized mAb sample (F3). The open symbols show the height of the monomer peak (q = 0.16 Å^{-1}), while the filled symbols show the height of the cluster peak (q = 0.10 Å^{-1}). These peak positions are indicated in the inset, which shows the evolution of the SANS patterns of Formulation F1 with time (compare to Figure 5).

obtain the heat-stressed sample (F3), the regular lyophilized mAb formulation (F1) was held at 110 °C for 5 h to generate about 15% aggregates after reconstitution, compared to about 6% aggregates in the regular formulation (Table 1), as detected by size-exclusion chromatography (SEC). Figure 8 is similar to that for the mAb in the deuterated sugar (F2, Figure 6a) but records the peak heights of the monomer (open symbols, at q = 0.16 Å^{-1}) and cluster (filled symbols, at q = 0.10 Å^{-1}) peaks separately. Peak heights are normalized by the heights of the monomer peaks of the two formulations to account for small differences in sample mass. Note that the peak positions correspond to those observed for F2 (Table 2) and that the cluster peak overtakes the monomer peak about 10 h after the start of the D_2O-rich vapor flow, indicating the presence of aggregates in both formulations after exposure to humidity.

If the aggregates detected by SEC were already present in the solid-state formulation before reconstitution, the cluster peak would be present in the VC-SANS patterns from the onset of the experiment or at least at short time scales. However, the fact that the cluster peak does not appear at the onset, especially for the heat-stressed formulation, and the fact that the peak heights align at early times for both formulations show that the irreversible aggregates detected by SEC are not present initially in the solid-state formulation. Specifically, the fact that the two formulations have the same peak heights even though they have significantly different aggregate content after reconstitution indicates that the formation of these reversible aggregates in the solid state is not directly related to the formulation's tendency to form aggregates in solution. However, the small increase in peak height of the stressed formulation as compared to the unstressed formulation toward the end of D_2O exposure could reflect its higher tendency to aggregate. These observations suggest that while modifications to the protein that make it prone to aggregation, such as partial unfolding or chemical modification, occur in the solid state, the proteins in stressed formulations are not aggregated in the solid state, where diffusion is quenched, but rather aggregate only upon reconstitution.

If the formation of the clusters observed by VC-SANS is not directly linked to the aggregates detected by SEC, what is the nature of these clusters in the solid state? If the aggregates detected by VC-SANS are irreversible, which would indicate a permanent loss of stability, they are expected to persist through reconstitution and also be detected by SEC. However, if SEC does not detect the aggregates formed during VC-SANS, they are reversible and presumably disassociate during the reconstitution process. Since the aggregate content of the reconstituted formulations before and after VC-SANS is the same (Figure 9), most clusters detected by VC-SANS appear to

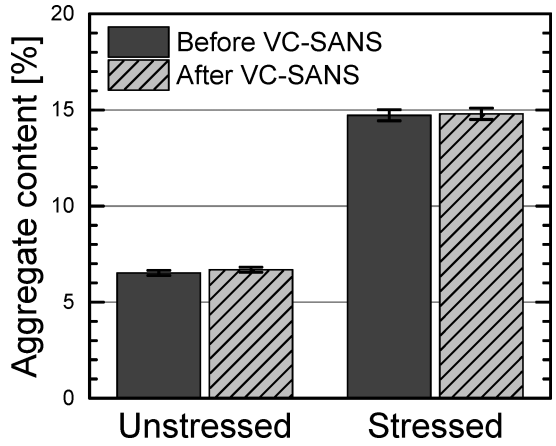

Figure 9. Comparison of aggregate content before and after exposure to vapor cell conditions for a regular (F1) and heat-stressed lyophilized mAb sample (F3), as measured by size-exclusion chromatography after reconstitution of the solid-state powders. Error bars correspond to one standard deviation.

be reversibly self-associating aggregates (reversible clusters). The fact that both formulations have the same peak height indicates that such aggregates are reversible. Although these aggregates disassociate upon reconstitution within a period of days after the VC-SANS experiment, their behavior when kept in the solid state over a longer span of time is an interesting topic for future study. For example, one could hypothesize that these reversible aggregates are precursors for irreversible aggregation during long-term storage and that formulations that exhibit such reversible aggregates after drying, e.g., due to low excipient concentrations, are more prone to long-term stability issues.

While these results demonstrate that VC-SANS is a useful tool in understanding protein-scale microstructural changes in solid-state formulations, it remains challenging to determine a formulation's long-term stability. However, recent reports have shown that measurements of molecular dynamics in these formulations are capable of predicting stability. For example,

DOI: 10.1021/acs.molpharmaceut.8b00935
Mol. Pharmaceutics 2019, 16, 173−183

both solid-state hydrogen−deuterium exchange with mass spectrometry (ssHDX-MS) and neutron backscattering (NB), techniques that probe different but potentially related fast protein dynamics, have been shown to reveal characteristics that correlate with long-term stability measurements.[6,10,22−25] However, the fundamental mechanisms of why these characteristics are good predictors are not yet fully understood. As VC-SANS combines aspects of both ssHDX-MS and NB by combining hydrogen−deuterium exchange with protein-scale characterization, it is a promising technique to help elucidate the basis for the correlations between long-term formulation stability and molecular dynamics.

4. CONCLUSIONS

VC-SANS with contrast variation is shown as a new method for characterizing changes to the molecular arrangement in situ on protein length scales in solid-state biopharmaceutical formulations. Investigation of lyophilized and spray-dried formulations shows crowded morphologies similar to those in frozen protein solutions, in which protein molecules are separated sufficiently to be stabilized by a protective sugar layer, independent of the drying method. Plasticization of the solid matrix through exposure to humidity leads to the formation of reversibly self-associated aggregates, possibly in the form of protein dimers, which dissociate after reconstitution. In addition, heat-stressed formulations do not show an increase in protein clustering in the solid state as compared to unstressed formulations, although the aggregate content of heat-stressed formulations after reconstitution is significantly higher. These results suggest that irreversible protein aggregation occurs upon reconstitution of the solid-state formulations, but that the formation of these aggregates is not directly caused by the presence of reversible aggregates in the solid state.

■ ASSOCIATED CONTENT

Supporting Information

The Supporting Information is available free of charge on the ACS Publications website at DOI: 10.1021/acs.molpharmaceut.8b00935.

Videos of the evolution of the scattering patterns with time for each of the formulations (ZIP)

Full q-range scattering patterns for Formulations F2 and F5 (PDF)

■ AUTHOR INFORMATION

Corresponding Author

*E-mail: lenhoff@udel.edu; Phone: +1 302 831 8989.

ORCID

Stijn H. S. Koshari: 0000-0002-0970-8991

Karthikan Rajagopal: 0000-0002-9398-4672

Yun Liu: 0000-0002-0944-3153

Norman J. Wagner: 0000-0001-9565-619X

Abraham M. Lenhoff: 0000-0002-7831-219X

Notes

The authors declare no competing financial interest.

■ ACKNOWLEDGMENTS

The financial support of Genentech Inc. is gratefully acknowledged. The authors thank Debby Chang and Graham Magill at Genentech for help with sample preparation and acknowledge the support of the National Institute of Standards and Technology (NIST), U.S. Department of Commerce, in providing the neutron research facilities used in this work. The statements, findings, conclusions, and recommendations are those of the authors and do not necessarily reflect the view of NIST or the U.S. Department of Commerce. Certain commercial equipment, instruments, or materials (or suppliers, or software, etc.) are identified in this paper to foster understanding. Such identification does not imply recommendation or endorsement by NIST nor does it imply that the materials or equipment identified are necessarily the best available for the purpose. Y.L. acknowledges the support by the Center for High Resolution Neutron Scattering (CHRNS), a partnership between the National Institute of Standards and Technology and National Science Foundation (NSF) under Agreement No. DMR-1508249. Microscopy access was supported by grants from the NIH-NIGMS (P20 GM103446), the NSF (IIA-1301765), and the State of Delaware.

■ REFERENCES

(1) Abdul-Fattah, A. M.; Truong-Le, V.; Yee, L.; Nguyen, L.; Kalonia, D. S.; Cicerone, M. T.; Pikal, M. J. *J. Pharm. Sci.* **2007**, *96* (8), 1983−2008.

(2) Gikanga, B.; Turok, R.; Hui, A.; Bowen, M.; Stauch, O. B.; Maa, Y.-F. *PDA J. Pharm. Sci. Technol.* **2015**, *69* (1), 59−73.

(3) Bowen, M.; Armstrong, N.; Maa, Y.-F. *J. Pharm. Sci.* **2012**, *101* (12), 4433−4443.

(4) Bowen, M.; Turok, R.; Maa, Y.-F. *Drying Technol.* **2013**, *31* (13−14), 1441−1450.

(5) Chang, D. P.; Garripelli, V. K.; Rea, J.; Kelley, R.; Rajagopal, K. *J. Pharm. Sci.* **2015**, *104* (10), 3404−3417.

(6) Cicerone, M. T.; Pikal, M. J.; Qian, K. K. *Adv. Drug Delivery Rev.* **2015**, *93*, 14−24.

(7) Pikal, M. J.; Rigsbee, D.; Roy, M. L.; Galreath, D.; Kovach, K. J.; Wang, B.; Carpenter, J. F.; Cicerone, M. T. *J. Pharm. Sci.* **2008**, *97* (12), 5106−5121.

(8) Park, J.; Nagapudi, K.; Vergara, C.; Ramachander, R.; Laurence, J. S.; Krishnan, S. *Pharm. Res.* **2013**, *30* (4), 968−984.

(9) Mensink, M. A.; Frijlink, H. W.; van der Voort Maarschalk, K.; Hinrichs, W. L. J. *Eur. J. Pharm. Biopharm.* **2017**, *114*, 288−295.

(10) Moorthy, B. S.; Zarraga, I. E.; Kumar, L.; Walters, B. T.; Goldbach, P.; Topp, E. M.; Allmendinger, A. *Mol. Pharmaceutics* **2018**, *15* (1), 1−11.

(11) Koshari, S. H. S.; Ross, J. L.; Nayak, P. K.; Zarraga, I. E.; Rajagopal, K.; Wagner, N. J.; Lenhoff, A. M. *Mol. Pharmaceutics* **2017**, *14* (2), 546−553.

(12) Devineni, D.; Gonschorek, C.; Cicerone, M. T.; Xu, Y.; Carpenter, J. F.; Randolph, T. W. *Eur. J. Pharm. Biopharm.* **2014**, *88* (2), 332−341.

(13) Xu, Y.; Grobelny, P.; Von Allmen, A.; Knudson, K.; Pikal, M.; Carpenter, J. F.; Randolph, T. W. *J. Pharm. Sci.* **2014**, *103* (5), 1356−1366.

(14) Patapoff, T. W.; Esue, O. *Pharm. Dev. Technol.* **2009**, *14* (6), 659−664.

(15) Svergun, D. I.; Koch, M. H. J. *Rep. Prog. Phys.* **2003**, *66* (10), 1735−1782.

(16) Grillo, I. In *Soft-Matter Characterization*; Borsali, R., Pecora, R., Eds.; Springer Netherlands: Dordrecht, 2008; pp 723−782.

(17) Hammouda, B. *Probing Nanoscale Structures — The SANS Toolbox*; National Institute of Standards and Technology: Gaithersburg, MD, 2010.

(18) Sivia, D. S. *Elementary Scattering Theory: For X-ray and Neutron Users*, 1st ed.; Oxford University Press: New York, 2011.

(19) Castellanos, M. M.; McAuley, A.; Curtis, J. E. *Comput. Struct. Biotechnol. J.* **2017**, *15*, 117−130.

DOI: 10.1021/acs.molpharmaceut.8b00935
Mol. Pharmaceutics 2019, 16, 173−183

(20) Castellanos, M. M.; Clark, N. J.; Watson, M. C.; Krueger, S.; McAuley, A.; Curtis, J. E. *J. Phys. Chem. B* **2016**, *120* (49), 12511−12518.
(21) Curtis, J. E.; Nanda, H.; Khodadadi, S.; Cicerone, M.; Lee, H. J.; McAuley, A.; Krueger, S. *J. Phys. Chem. B* **2012**, *116* (32), 9653−9667.
(22) Sophocleous, A. M.; Zhang, J.; Topp, E. M. *Mol. Pharmaceutics* **2012**, *9* (4), 718−726.
(23) Moorthy, B. S.; Schultz, S. G.; Kim, S. G.; Topp, E. M. *Mol. Pharmaceutics* **2014**, *11* (6), 1869−1879.
(24) Qian, K. K.; Grobelny, P. J.; Tyagi, M.; Cicerone, M. T. *Mol. Pharmaceutics* **2015**, *12* (4), 1141−1149.
(25) Wang, B.; Tchessalov, S.; Cicerone, M. T.; Warne, N. W.; Pikal, M. J. *J. Pharm. Sci.* **2009**, *98* (9), 3145−3166.
(26) Shelton, C. K.; Jones, R. L.; Dura, J. A.; Epps, T. H. *Macromolecules* **2016**, *49* (19), 7525−7534.
(27) Kline, S. R. *J. Appl. Crystallogr.* **2006**, *39* (6), 895−900.
(28) Yearley, E. J.; Godfrin, P. D.; Perevozchikova, T.; Zhang, H.; Falus, P.; Porcar, L.; Nagao, M.; Curtis, J. E.; Gawande, P.; Taing, R.; Zarraga, I. E.; Wagner, N. J.; Liu, Y. *Biophys. J.* **2014**, *106* (8), 1763−1770.
(29) Winther, L. R.; Qvist, J.; Halle, B. *J. Phys. Chem. B* **2012**, *116* (30), 9196−9207.
(30) Sophocleous, A. M.; Topp, E. M. *Mol. Pharmaceutics* **2012**, *9* (4), 727−733.
(31) Godfrin, P. D.; Zarraga, I. E.; Zarzar, J.; Porcar, L.; Falus, P.; Wagner, N. J.; Liu, Y. *J. Phys. Chem. B* **2016**, *120* (2), 278−291.

DOI: 10.1021/acs.molpharmaceut.8b00935
Mol. Pharmaceutics 2019, 16, 173−183